Skin Effects in Narrow Copper Microstrip at 77 K

UTTAM S. GHOSHAL, MEMBER, IEEE, AND LAWRENCE N. SMITH, MEMBER, IEEE

Abstract—We have performed finite element and circuit simulations to analyze the performance of copper polyimide wafer scale interconnects at 77 K as a function of line width, dielectric thickness, and line length. The copper line width was generally kept equal to the dielectric thickness; this is a realistic geometry which gives a characteristic impedance of about 60 Ω, but one which is difficult to analyze using analytical techniques. The finite element simulations were used to extract the frequency-dependent complex impedance which arises from the normal skin effect. This was then fitted to obtain an equivalent circuit which could be used in SPICE simulations. Anomalous skin effect was determined to be unimportant for frequencies below 20 GHz and was not included in the detailed finite element models. We have used these results to analyze the performance of these lines for digital interconnects and to identify possible applications that would benefit from still lower resistance, such as might be obtainable from the high temperature oxide superconductors. Skin effects were determined to be important for predicting the response for times less than 1.2 times the time of flight delay, while for larger instants the dc resistance corresponding to the cross section of the signal line is adequate.

I. INTRODUCTION

LIQUID NITROGEN temperature (77 K) operation of CMOS VLSI circuits has recently been introduced for high-performance mainframe computers [1]. Among the major advantages are smaller system volume, better computing speed, and higher reliability. There exists a wide variety of III–V devices such as HEMT's, HBT's, and even Si bipolar transistors [2] which have very high gain characteristics at 77 K and could be used, possibly in conjunction with CMOS, to drive signals through interconnects at high speeds. Wafer scale packaging technologies, such as the copper polyimide "medium film" technology [3], [4], are now becoming mature enough to provide dense interconnects and efficiently pack chips at the first level of system interconnections. The interconnect lengths in these technologies are typically around 10 cm, although they may be as long as 50 cm in some special cases. The recent discoveries of high temperature superconductivity in oxide materials [5], [6] with critical temperatures in the 90 K regime and possibility of superconducting devices at 77 K have led many to believe that replacement of copper conductors by superconductors in wafer scale interconnects might remove important constraints on signal delay, attenuation, and dispersion in off-chip communication, especially as interconnects are scaled to finer geometries to provide more intrachip communication paths.

Manuscript received April 1, 1988; revised July 25, 1988.

The authors are with the Microelectronics and Computer Technology Corporation, Austin, TX 78727.

IEEE Log Number 8824165.

Our work is different from the earlier, seminal work by Kautz [7] and recent literature [8], [9] in three important regards. First, we use a narrow microstrip geometry with the signal line embedded in the dielectric such that the distance of the signal line from the ground plane equals its width and the signal line thickness equals half its width. This results in a characteristic impedance of about 60 Ω at high frequencies when used with polyimide dielectric which has a dielectric constant of 3.5. The line widths considered are all below 10 μm, in accordance with future trends forecast by industry experts in this technology. The geometry is difficult to analyze analytically because it is dominated by fringing fields, but is technologically more important than the low-impedance, wide-microstrip geometry considered by Kautz, which ignores fringing fields. Such low impedance lines would place too high a demand on driver size, power consumption, and switching transients in practical digital applications. Second, we calculate an equivalent circuit for the lines using multiple inductors and resistors by fitting to the frequency-dependent complex impedance obtained from our finite element simulations. Third, we then simulate the line response for a variety of different circuit configurations and inputs using SPICE [10], including step functions with finite rise time and matched source impedance, and scaled CMOS drivers. This is more relevant than the Gaussian pulse propagation which has been previously analyzed using an analytic approach. We present simple physical interpretations of these simulations, discuss the circumstances under which the skin effect can be neglected, and comment on possible windows of opportunity for superconducting interconnects.

Hilbert *et al.* [11] have considered the possible need for superconducting interconnect by exploring the line response for various widths, lengths, and driver impedances. They make the simplifying assumption that skin effects can be ignored, and model a short segment of the transmission line by a simple resistor in series with a lossless line. The resistance is assumed to be the dc resistance for the cross section of the line, while the characteristic impedance of the lossless line is the TEM impedance, which assumes that the currents are constrained to the surface. Both these assumptions need to be analyzed by comparing their results with the exact calculations. For frequency components in which the skin depth $\delta = \sqrt{2/\omega\mu\sigma}$ is smaller than the line thickness, the effective resistance

0018-9480/88/1200-1788$01.00

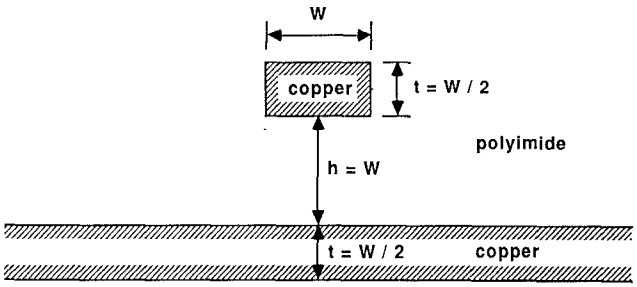

Fig. 1. The microstrip geometry analyzed by finite element simulations for obtaining skin effect impedances from 0 to 10 GHz. The conductivity of copper at 77 K is assumed to be 450 (S/μm) and the relative dielectric constant of the polyimide dielectric was assumed to be 3.5. A high-T_c superconductor substitute for copper with parameters σ_{nn} = 0.2 (S/μm), $\beta = 1$, $\lambda_0 = 0.1$ μm, and $T_c = 90$ K was also analyzed based on the phenomenological two-fluid model.

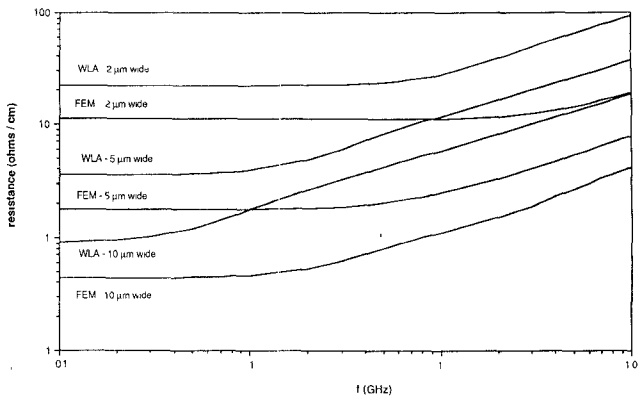

Fig. 2. The variation of resistance of copper interconnects as a function of frequency for different widths as obtained from finite element simulations and the wide line approximation used by Kautz [7]. The interconnect geometry is shown in Fig. 1.

should be higher than the dc resistance. For copper at 77 K, δ is only about 0.75 μm at 1 GHz and scales inversely as the square root of frequency. A more difficult question is the treatment of the ground plane in the narrow stripline case under consideration, because the currents will be relatively spread out compared with the signal line. The degree to which the currents spread out will also increase as the frequency is lowered to dc, limited only by the actual extent of the ground plane. This leads to a frequency-dependent inductance, resistance, and characteristic impedance.

We have not incorporated the anomalous skin effect into our finite element model. This is important when the classical skin depth δ is much smaller than the electronic mean free path l_e, leading to a nonlocal relation between the current density $\boldsymbol{J}$ and the electric field $\boldsymbol{E}$. For copper at 77 K with conductivity $\sigma = 450$ (S/μm), the mean free path can be calculated from the material constant $(\sigma/l_e) = 1.55 \times 10^{15}$ $\Omega^{-1}\mathrm{m}^{-1}$ [12]. Thus $\delta \geq l_e$ ($= 0.29$ μm) for frequencies $f \leq 6.6$ GHz. This neglect of anomalous skin effect is further justified in Appendix I, where it is shown that for a wide line it makes less than 1 percent difference at 1 GHz, 5.7 percent difference at 10 GHz, and about 9.8 percent difference at 20 GHz. The frequency range under consideration in this paper is adequate for most digital applications, for which rise times correspond to 50 ps or greater.

II. Simulation Approach

We have developed in-house techniques to analyze the frequency-dependent impedances of general 2-D and 3-D lossy interconnects, using finite element techniques. There are many sophisticated finite element software packages, such as ANSYS [13], for analysis of thermomechanical problems; our work has been to cast the electromagnetic problem into a form which can make use of these packages. In this section we briefly describe our method (see also [14]).

The microstrip geometry is shown in Fig. 1. We assumed a copper conductivity of 450 (S/μm) at 77 K; this is a value we have measured for electroplated copper and is close to bulk values. The conductivity for the same material was measured to be 58 (S/μm) at 300 K. The relative dielectric constant of the polyimide was assumed to be 3.5. The simulation we perform corresponds to driving a short differential segment of the line with a voltage step while the end of the line is mathematically shorted. The skin parameters are calculated by solving the partial differential equation for the time evolution of the magnetic vector potential $\boldsymbol{A}$: $-\nabla^2 \boldsymbol{A} + \sigma\mu(\partial \boldsymbol{A}/\partial t) + \mu\epsilon(\partial^2 \boldsymbol{A}/\partial t^2) = \boldsymbol{J}_0$. Proper current continuity and boundary conditions were applied to maintain current conservation and ensure that the fields decay to zero at large distances. The impedances as a function of frequency are obtained from the current–voltage definitions based on power and energy considerations [15] and then fitted a linear circuit consisting of a series array of parallel resistor–inductor segments. This equivalent circuit can then be used in SPICE or equivalent circuit simulation programs to simulate the transmission line response in complex circuits. The frequency we use extends from low frequencies up to about 10 GHz. This upper limit is somewhat artificial: the method can be extended to much higher frequencies, but would require finer spatial resolution and increased computer time and expense. The upper frequency limit was chosen to be 10 GHz because higher frequency components are not important in determining the propagation characteristics of digital signals when the pulse rise times are greater than 50 ps. Beyond 10 GHz, the skin effect is well developed and can be calculated from the geometrical factor discussed in Section IV. Capacitances were computed by solving the Laplace's equation for the scalar electric potential in the dielectric region using finite elements, with conductor boundaries subjected to fixed potentials (Dirichlet boundary conditions).

III. Simulation Results

Impedances were obtained for the line geometry shown in Fig. 1. We started with the "nominal" present-day geometry of 10-μm-wide and 5-μm-thick lines with 10-μm-thick dielectric and also considered the same geometry

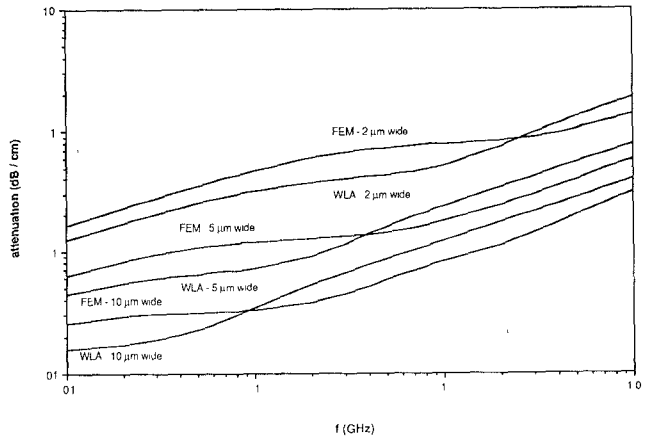

Fig. 3. The attenuation of signals propagating through copper interconnects as a function of frequency for different widths as obtained from finite element simulations and the wide line approximation used by Kautz [7]. The interconnect geometry is shown in Fig. 1.

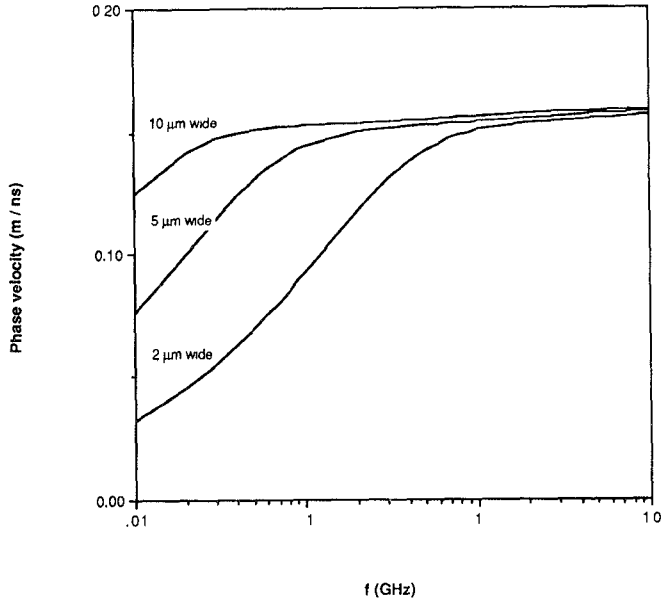

Fig. 4. The phase velocity of signals propagating through copper interconnects as a function of frequency for different widths as obtained from finite element simulations. The interconnect geometry is shown in Fig. 1.

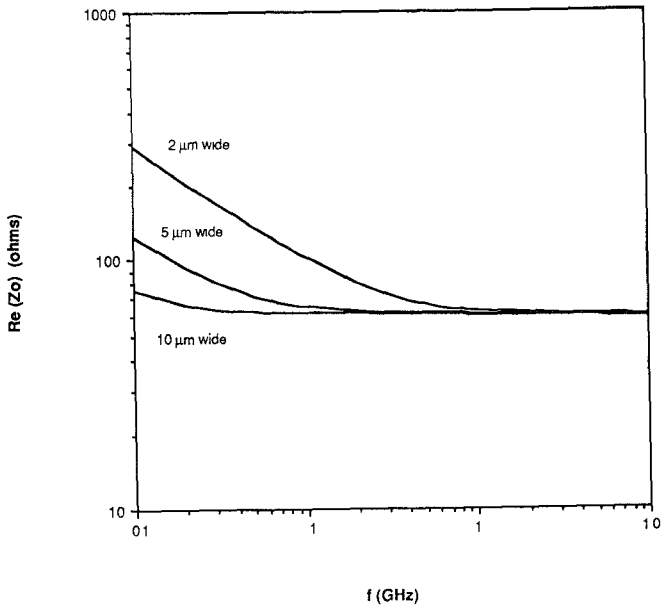

Fig. 5. The real part of the characteristic impedance of copper interconnects as a function of frequency for different widths as obtained from finite element simulations. The interconnect geometry is shown in Fig. 1.

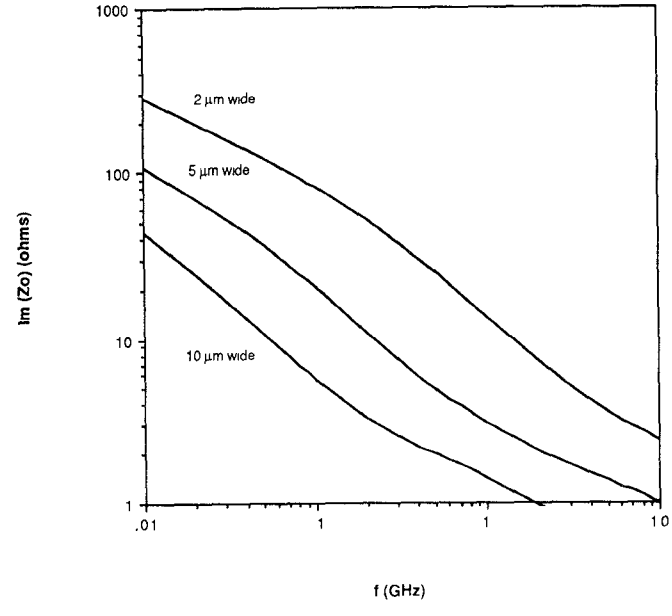

Fig 6. The imaginary part of the characteristic impedance of copper interconnects as a function of frequency for different widths, as obtained from finite element simulations. The interconnect geometry is shown in Fig. 1.

scaled by a factor of 2 and 5. Results from the finite element simulations for the resistances of such interconnects as a function of frequency and the ones obtained by the wide line approximation (WLA) used by Kautz [7] are shown in Fig. 2. Figs. 3 and 4 show the variation of attenuation per unit length $\alpha = (20\log_{10} e)\,\mathrm{Re}(\gamma)$ and phase velocity $v_r = 2\pi f/\mathrm{Im}(\gamma)$ as a function of frequency, γ being the propagation constant for the frequency f. Figs. 5 and 6 show the real and imaginary parts of the complex characteristic impedance Z_0 as a function of frequency.

In addition to the above results, which were based on the finite element simulations, we calculated the surface impedance due to the anomalous skin impedance based on the theory of Reuter and Sondheimer [16] (see Appendix I). Fig. 7 shows the real and imaginary parts of the surface impedance (both normal and anomalous) for wide copper microstrips as a function of frequency. Figs. 8 and 9 show the variation of the surface impedance and line attenuation of a high-T_c superconductor over 0–10 GHz assuming the following parameters: $\sigma_{nn} = 0.2(\mathrm{S}/\mu\mathrm{m})$, $\beta = 1$, $\lambda_0 = 0.1$ μm, $T_c = 90$ K. These results were based on the model and assumptions outlined in Appendix II.

The next set of results are meant to evaluate the performance of copper interconnects in digital wafer scale circuits at 77 K. The linearized circuit representation of a 1.0-cm-long transmission line segment is shown in Fig. 10.

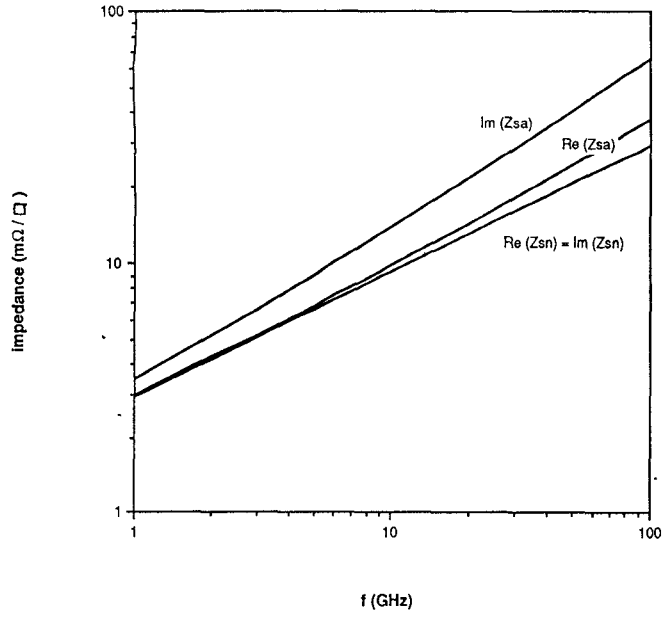

Fig. 7. Anomalous skin impedance Z_{sa} and normal skin impedance as a function of frequency for a copper half-plane at 77 K. The mean free path of the electrons was assumed to be 0.29 μm. The normal skin impedance Z_{sn} has its real part equal to the imaginary part for all frequencies.

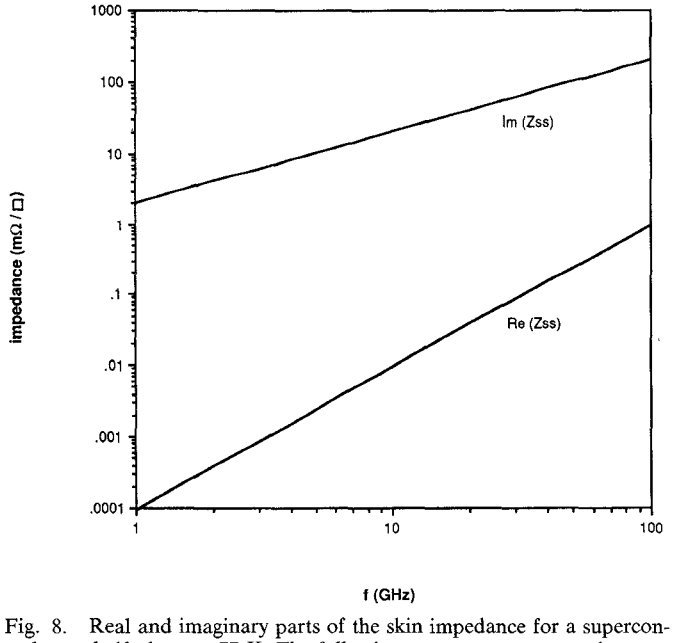

Fig. 8. Real and imaginary parts of the skin impedance for a superconductor half-plane at 77 K. The following parameters were used: $\sigma_{nn} = 0.2$ (S/μm), $\beta = 1$, $\lambda_0 = 0.1$ μm, $T_c = 90$ K, $G = 1$.

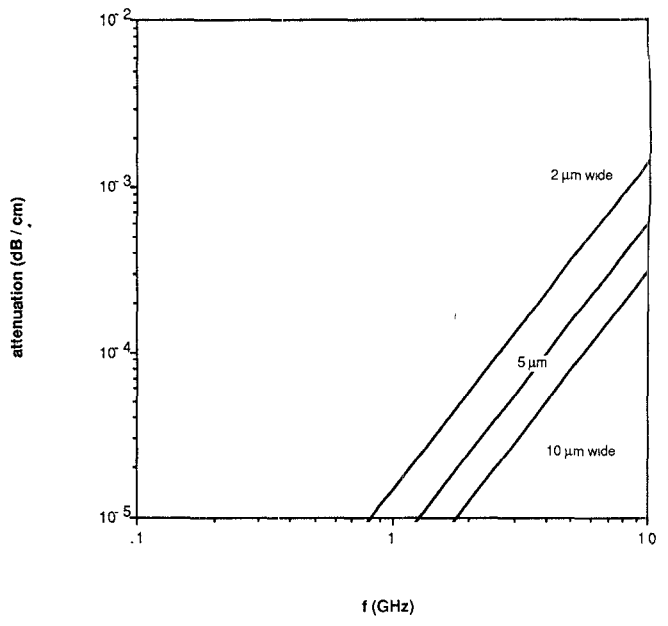

Fig. 9. The attenuation of signals propagating through a high-T_c superconductor as a function of frequency for different widths, as obtained from the two-fluid model discussed in Appendix II. The interconnect geometry is shown in Fig. 1.

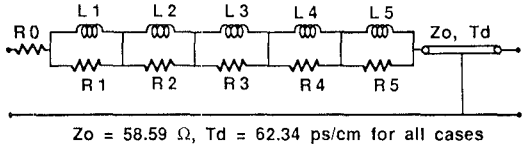

Case	10 μm x 5 μm	5 μm x 2.5 μm	2 μm x 1 μm
R0 (Ω/cm)	0.45	1.77	11.1
R1 (Ω/cm)	0.46	1.11	9.11
L1 (nH/cm)	0.14	0.18	0.19
R2 (Ω/cm)	0.32	3.57	9.45
L2 (nH/cm)	0.08	0.12	0.09
R3 (Ω/cm)	1.60	6.44	0
L3 (nH/cm)	0.06	0.07	0
R4 (Ω/cm)	1.93	0	0
L4 (nH/cm)	0.04	0	0
R5 (Ω/cm)	2.41	0	0
L5 (nH/cm)	0.02	0	0

Fig. 10. The linear circuit model for 1-cm-long lossy copper interconnects at 77 K obtained by regression fitting over 0–10 GHz to the real and imaginary parts of the line impedances calculated from finite element simulations. This circuit was used in SPICE [10] to simulate transmission line circuits.

This circuit was obtained by regression-fitting the linear impedance function to the real and imaginary parts of the impedance obtained by finite element simulations and has less than 5 percent error between 0 and 10 GHz. The linearization procedure is discussed in greater detail by Tripathi and Hill [23]. Fig. 11 shows the two circuit configurations investigated using SPICE; the first configuration consists of the lossy transmission line with linear matched source and open far end and the second configuration has a nonlinear mismatched CMOS driver ($\beta_p = 350$, $\beta_n = 175$) instead of the linear source. The far ends of the transmission lines were kept open because most CMOS or BiCMOS circuits (which generally have driver output impedances greater than the transmission line characteristic impedance) currently designed adopt this approach. The SPICE parameters chosen corresponded to an advanced 0.5 μm technology [17] with a large signal transconductance (i.e., transconductance at $V_{ds} = V_{gs} =$

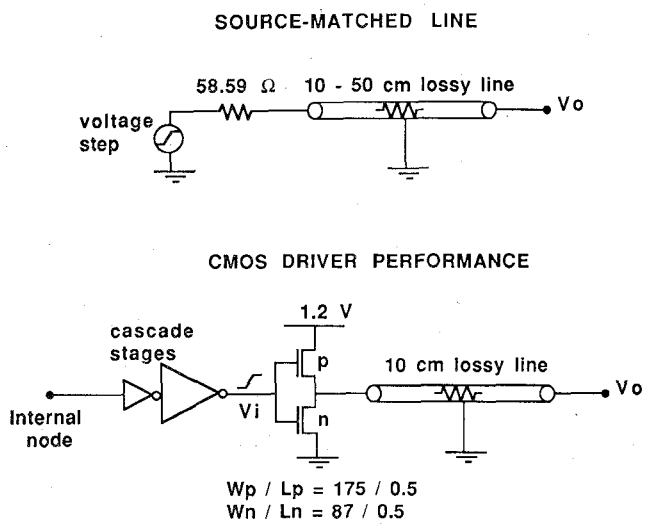

Fig. 11. Two circuit configurations used to evaluate the performance of copper interconnects in digital wafer scale circuits at 77 K.

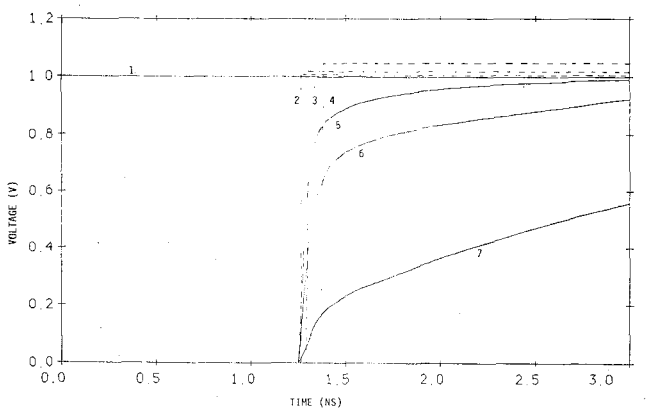

Fig. 12. The signal response at the receiver end of a 20 cm transmission line. Curve 1 is the input voltage step waveform. Curves 2, 3, and 4, represented by dashed lines, represent the response on 10 μm, 5 μm, and 2 μm wide superconductors as predicted by the two-fluid model. Solid curves 5, 6, and 7 correspond to the response on 10 μm, 5 μm, and 2 μm wide copper interconnects at 77 K as predicted by the linear circuit extracted from the finite element simulations.

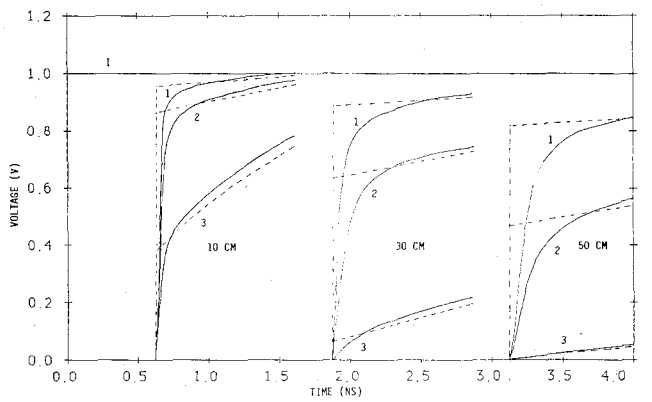

Fig. 13. The signal response at the receiver end of the copper lines for three different line lengths: 10 cm, 30 cm, and 50 cm. Solid curves 1, 2, and 3 show the response obtained by including skin effects for 10 μm, 5 μm, and 2 μm wide copper lines at 77 K. The curves represented by dashed lines show the corresponding curves obtained by neglecting the *RL* circuits due to skin effect but retaining the dc resistance of the interconnects. Curve I represents the input voltage step waveform. The response obtained by neglecting skin effect closely follows the exact response for instants greater than 1.2 times the time of flight delay.

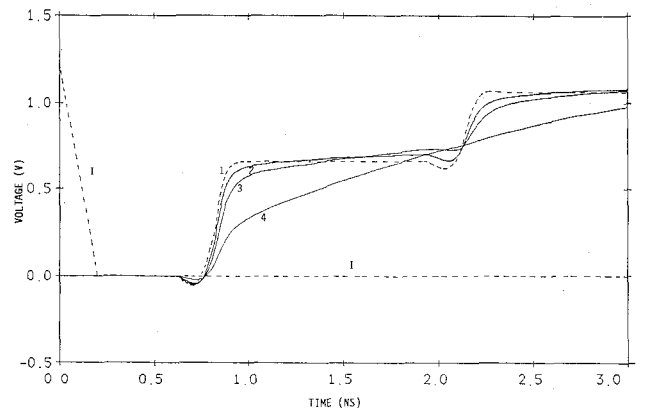

Fig. 14. The signal response at the receiver end of a 10-cm-long copper line driven by a CMOS driver at 77 K. Curve I represents the waveform at the input of the last stage of the cascade chain. Solid curves 2, 3, and 4 represent the response on 10 μm, 5 μm, and 2 μm wide copper interconnects whereas curve 1 corresponds to an ideal lossless line with the characteristic impedance $Z_{0\infty} = 58.59\ \Omega$ and delay per unit length = 62.34 ps/cm.

1.2 V) of 86 mS/mm for *n*-channel and 43 mS/mm for *p*-channel. Both the transistors had a threshold voltage of 0.3 V. An ideal step was chosen for the first configuration so as to compare the interconnect performance without the influence of any device technology. For the CMOS driver, the rise time of the input pulse at the last stage of the driver cascade was taken to be 0.2 ns. Fig. 12 shows the response of 20-cm-long copper lines at 77 K and compares it to the response expected using a high-T_c superconductor substitute for copper. Fig. 13 compares the response on copper lines of different lengths (10 cm, 30 cm, and 50 cm) calculated using the linearized circuit model, which included skin-effect to the one neglecting skin effect but retaining the d.c. resistance contribution due to the finite cross section of the signal conductor. Fig. 14 shows the effects of the nonlinear CMOS driver on the response of 10-cm-long copper interconnects at 77 K.

IV. Discussion

As can be inferred from Fig. 2, WLA [7] grossly overestimates the resistances—by a factor of 2 at d.c. frequencies and by a factor of 4 at higher frequencies. This is because at low frequencies, the ground plane resistance is zero, contrary to WLA, while at high frequencies there are additional conducting paths on the sides of the interconnects and the ground plane. At high frequencies, the resistance $R_{sn} = G/\sigma\delta$, where G is essentially a geometric factor independent of material parameters. This factor G is closely related to the shape factor discussed in [18] and [19]. To obtain an interpretation of G, we assume that fields decay exponentially from the surface into the conductor at high frequencies, in which case the general formula of resistance [15] based on a (I^2R/I^2)-type power

relation can be simplified as follows:

$$R_{sn} = \frac{\int_{C+G} \sigma |E|^2 \, dS}{\left| \int_{C/G} \sigma E \, dS \right|^2} \rightarrow \frac{1}{\sigma\delta} \frac{\int_{C+G} |E|^2 \, dl}{\left| \int_{C/G} E \, dl \right|^2} = \frac{G}{\sigma\delta} \quad \text{as } \omega \rightarrow \infty.$$

The integrals in the numerator are evaluated for the conductor as well as the ground plane, whereas the ones in the denominator are evaluated either for the conductor or the ground plane, because the current in the conductor is same as the current in the ground plane. The surface S is the cross-sectional surface and the contour l is the path bounding S. It can be directly inferred that for wide lines $G = (2/\text{width})$ and that G scales up by the scaling factor as the geometries are scaled down. From simulations it was found that the ground plane contributed about one third of the total resistance at high frequencies and $G \approx 0.05$ (μm^{-1}) for the nominal geometry. Simulation results indicate that at high frequencies the skin impedance of the copper interconnect per unit length closely follows the approximation $Z_{sn} = G\sqrt{j\omega\mu/\sigma} \coth(\sqrt{j\omega\mu\sigma}\, GWt)$, W being the width of the conductor and t the thickness.

The capacitance per unit length C is about 3.4 times greater than the capacitance in Kautz's case and the characteristic impedance at high frequencies, $Z_{0\infty}$, is 3.4 times lower. Fig. 3 shows the variation of attenuation α for sinusoidal signals as a function of frequency f. By definition, $\alpha = (20\log_{10} e)\,\text{Re}(\gamma)$, γ being the propagation constant for the frequency f. At high frequencies, $\alpha \approx (20\log_{10} e) R_{sn}/2Z_{0\infty}$; hence Kautz's results are 2 times greater. The line internal inductance increases at low frequencies roughly as $1/\sqrt{f}$ but the internal reactance decreases as $\sqrt{f}$. At very low frequencies (i.e., $f \rightarrow 0$), the contribution to α from the increase in the internal inductance is small and $\alpha \rightarrow (20\log_{10} e)\sqrt{\pi f R_{\text{dc}} C}$; hence Kautz's results are about 2.5 times lower.

Fig. 4 shows the variation of the phase velocity v_r as a function of frequency. At low frequencies, $v_r \rightarrow 2\sqrt{\pi f/R_{\text{dc}}C}$, whereas when $f \rightarrow \infty$ the phase velocity approaches the velocity of light in the medium. Similar conclusions can be derived for the characteristic impedance Z_0. Figs. 5 and 6 show that as $f \rightarrow 0$, both $\text{Re}(Z_0)$ and $|\text{Im}(Z_0)| \rightarrow \frac{1}{2}\sqrt{R_{\text{dc}}/\pi fC}$ and as $f \rightarrow \infty$, $\text{Re}(Z_0) \rightarrow Z_{0\infty}$ and $\text{Im}(Z_0) \rightarrow 0$. The low-frequency asymptotic values for α, v_r, and Z_0 hold good very near the d.c. condition, since there are corrections due to the increase in the internal inductance.

The effect of anomalous skin effect (Fig. 7) is negligible for the frequencies over which present digital circuits operate. For normal skin effect, the real part and the imaginary part of the surface impedance are the same ($=1/\sigma\delta$), but in the case of anomalous skin effect, the surface reactance is considerably greater than the surface resistance. This inductive term may be important in considering some special applications, but it seems to be small when compared to the inductance contribution from the external magnetic fields in the dielectric.

Superconductor surface impedance behavior (Fig. 8), based on the two-fluid model, has surface resistance increasing as the square of the frequency and the surface reactance scaling up proportional to the frequency. The attenuation α_{sc} for the superconducting lines (Fig. 9) also varies as $(20\log_{10} e)R_{ss}/2Z_0$ at high frequencies, although it is several orders of magnitude smaller than the attenuation in copper interconnects (Fig. 3). The attenuation α_{sc} scales up roughly by the scaling factor as the geometry is scaled down and increased as the square of the frequency. When compared to the external line impedances, the main contribution due to the internal impedance of the superconductor was an additional inductance which increased the characteristic impedance and the time of flight delay by a small amount as compared to an ideal lossless line. The ideal lossless line for the geometry shown in Fig. 1 would have a characteristic impedance of 58.59 Ω and would introduce a delay of 62.34 ps/cm in signal propagation. In comparison, the superconducting lines of widths 10 μm, 5 μm, and 2 μm have characteristic impedances of 59.76 Ω, 60.91 Ω, and 64.22 Ω, respectively. The corresponding delays are 63.59 ps/cm, 64.81 ps/cm, and 58.33 ps/cm.

The signal propagation characteristics for matched 20 cm lines (Fig. 12) with different cross sections clearly indicate that superconducting interconnects have an advantage over copper interconnects at 77 K in providing lower dispersion and delay when the nominal geometry is scaled by a factor of 2. The additional delay in the superconducting lines is a small penalty when compared to the attenuation and dispersion in lossy lines. In Fig. 13, when the skin effect terms are neglected, the leading edge of the signal at the receiver end is attenuated by $\exp(-(R_t/2Z_{0\infty}))$, R_t being the total line resistance. However when skin effect terms are included, the signal starts from zero level after the time of flight delay and quickly follows the approximate characteristics obtained by neglecting the skin effect. In all our circuit simulations, skin effects were determined to be important for predicting the response for times less than 1.2 times the time of flight delay, while for larger instants the approximation obtained by neglecting skin effects did yield characteristics which were in close agreement with the exact results. This justifies the assumption made by Hilbert *et al.* [11] to study the system implications of superconducting interconnects.

Signal propagation characteristics in the case of the CMOS driver at 77 K are very similar to the previous results. The source impedance of the driver is roughly 117 Ω and this results in the mismatched characteristics and reflections shown in Fig. 14. The response is just sufficient for first instance switching at the receiver end, especially if there is a Schmitt trigger on the receiver chip. Even though an additional delay penalty of the order of 0.3 ns is paid in the initial stages of the driver cascade, the basic conclusions on the interconnect performance remained the same. The SPICE parameters chosen for CMOS are very conservative and improvements by a factor of 2 in transconductance may be obtained by optimizing the device design.

without changing the channel length. Low-temperature CMOS with 0.5 μm will thus clearly represent a high-speed device technology for computer applications in the near future. The internal driver delay could be substantially less in the nm MOSFET technologies [20] or heterojunction devices if high-performance silicon bipolar devices [2] were available.

V. Conclusions

Copper wafer scale interconnects at 77 K provide performance comparable to superconductors even when the present-day interconnect densities are scaled by a factor of 2. However, beyond this limit, as the need for higher densities for the first level of system interconnects grows and higher performance devices are available, superconductors will play an increasingly important role in alleviating the constraints imposed by signal attenuation and dispersion. We have analyzed in detail the signal propagation through single lines of different cross sections and lengths by including normal skin effect and effects of fringing fields. Calculation of crosstalk without neglecting skin effect, power distribution systems, etc., needs to be analyzed before an unqualified recommendation for the use of superconductors in digital systems can be made. Superconducting lines could have a direct impact on interconnect dominated neural networks and in providing idealized multiphase timing clocks for synchronizing different functional components in a ULSI system. Another possible area of impact is in providing low d.c. drops in power distribution circuits. However, the high-T_c superconducting technology is in its infant stage and is plagued by several fabrication difficulties. Loss mechanisms and even the basic physics in these oxides are not well understood. Achieving small penetration depths and high current densities is difficult, even though considerable progress has already been made. There also exists the possibility of interfacing high-gap junctions to low-voltage FET's in a hybrid superconductor–semiconductor system. Cost/performance figures are high now but will certainly be competitive in future.

Appendix I
Anomalous Skin Effect

When the skin depth δ is comparable to the electronic mean free path l_e, the relation between the current density and the electric field at any point for an isotropic metal assumes the nonlocal form proposed by Pippard [16]:

$$\boldsymbol{J}(\boldsymbol{r}) = \frac{3\sigma}{4\pi l_e}\int_V (\boldsymbol{r}-\boldsymbol{r}')((\boldsymbol{r}-\boldsymbol{r}') \cdot \boldsymbol{E}(\boldsymbol{r}'))|\boldsymbol{r}-\boldsymbol{r}'|^{-4} e^{-|\boldsymbol{r}-\boldsymbol{r}|/l_e}\, d^3\boldsymbol{r}'.$$

The integral here is evaluated for the entire volume. Assuming diffuse scattering and specular reflection at the surface, Reuter and Sondheimer [16] solved the equations and derived the following formula for the anomalous skin impedance Z_{sa} of a conductor half-plane:

$$Z_{sa} = \frac{2\pi j l_e}{\sigma\delta^2}\left[\int_0^\infty \ln\left\{1+3j(l_e/\delta)\frac{2\left((1+t^2)\tan^{-1}t - t\right)}{t^5}\right\} dt\right]^{-1}$$

The anomalous skin impedance was evaluated using this formula and compared to the normal skin impedance. The integration was performed by first transforming the integral so that it is defined between finite limits, 0 and 1, and then using a midpoint integration scheme. Fig. 7 shows the comparison of the skin impedance Z_{sa} with the normal skin impedance as a function of frequency. The anomalous skin resistance is greater than the normal skin resistance by 0.96 percent at 1 GHz, 3.21 percent at 5 GHz. 5.7 percent at 10 GHz, and 9.80 percent at 20 GHz.

Appendix II
Superconducting Line Parameters

The calculations of the performance of a high-T_c superconductor–polyimide system were based on the two-fluid model [21], [22] which is similar to [8] but corrected for finite geometry. Such a phenomenological approach is used because the underlying physics of the high-T_c superconductor is not well understood. The conductivity of the superconductor $\sigma_{ss} = (\sigma_n - j\sigma_s)$ is the sum of the contributions from normal current (quasiparticles) and supercurrent (Cooper pairs):

$$\sigma_n = \sigma_{nn}\left(\frac{T}{T_c}\right)^\beta$$

σ_{nn} being the normal conductivity at the critical temperature T_c, and

$$\sigma_s = \frac{\left(1-\left(\frac{T}{T_c}\right)^\beta\right)}{\omega\mu\lambda_0^2}$$

where $\lambda_0 = \sqrt{\hbar/(\pi\mu\sigma_m\Delta(0))}$, $\Delta(0)$ being the energy gap. Here β is a parameter such that $1 \leqslant \beta \leqslant 4$.

If the penetration depth of the field is small (≈ 0.2 μm), the internal impedance due to the superconductor is given by $Z_s = G\sqrt{(j\omega\mu\sigma_{ss})}$, where G is a constant dependent on the geometry of the interconnects. If the fields decay into the superconductor as $\exp(-\sqrt{j\omega\mu\sigma_{ss}})$ this factor G is the same as the quantity $(R_{sn}\sigma\delta)$ calculated from finite element simulations, R_{sn}, σ, and δ being, respectively, the resistance, conductivity, and skin depth in the case of copper conductors at high frequencies (≈ 10 GHz).

References

[1] Special Issue on Low Temperature Electronics. *IEEE Trans. Electron Devices*, vol. ED-34, no. 1, 1987.
[2] J. Stork *et al.*, in *IEEE IEDM Tech. Dig.*, 1987.
[3] R. Carlson and C. Neugebauer, *Proc. IEEE*, vol. 74, pp. 1741–1752, Dec. 1986.
[4] R. Jensen *et al*, *IEEE Trans Components, Hybrids, Manuf. Technol.*, vol. CHMT-7, no. 4. pp. 384–392. 1984.
[5] C. Chu *et al.*, *Phys. Rev Lett.*, vol. 58, no. 12, pp 405–408, 1987.

[6] R. J. Cava *et al.*, *Phys. Rev. Lett.*, vol. 58, no. 16, pp. 1676–1679, 1987.
[7] R. L. Kautz, *J. Res. Nat. Bur. Stand.*, vol. 84, no. 3, pp. 247–259, 1979.
[8] O. K. Kwon *et al.*, *IEEE Trans. Electron Device Lett.*, vol. EDL-8, no. 12, pp. 582–585, 1987.
[9] S. Tewksbury, L. Hornak, and M. Hatamian, *IEEE Trans. Electron Devices*, to be published.
[10] L. W. Nagel, ERL Memo ERL-M520, University of California, Berkeley, 1975.
[11] C. Hilbert, D. Herrell, and D. Gibson, *IEEE Trans. Electron Devices*, to be published.
[12] E. H. Sondheimer, *Advances in Phys.*, vol. 1, no. 1, pp. 1–42, 1952.
[13] G. DeSalvo and J. Swanson, *ANSYS Engineering System User's Manual*, vol. 1, Swanson Analysis Systems, 1986.
[14] U. Ghoshal, T-C Wang, and L. Smith, in *Proc. 4th Int. IEEE VLSI Multilevel Interconnect Conf.*, 1987, pp. 265–272.
[15] J. Brews, *IEEE Trans. Electron Devices*, vol. ED-33, pp. 1356–1365, Sept. 1986.
[16] G. Reuter and E. Sondheimer, *Proc. Roy. Soc.*, vol. A195, no. 12, pp. 336–364, 1948.
[17] J. Y.-C. Sun *et al.*, *IEEE Trans. Electron Devices*, vol. ED-36, pp. 19–27, Jan. 1987.
[18] H. A. Wheeler, *Proc. IRE*, vol. 30, pp. 412–424, 1942.
[19] P. Waldhow and I. Wolf, *IEEE Trans. Microwave Theory Tech.*, vol. MTT-33, pp. 1076–1081, 1985.
[20] G. Sai-Halasz *et al.*, *IEEE Electron Device Lett.*, vol. EDL-8, pp. 463–466, Oct. 1987.
[21] M. Tinkham, *Superconductivity*. New York: Gordon and Breach, 1965.
[22] T. Van Duzer and C. Turner, *Principles of Superconductive Devices and Circuits*. New York: Elsevier, 1981.
[23] V. Tripathi and A. Hill, *IEEE Trans. Microwave Theory Tech.*, vol. MTT-36, pp. 256–262, Feb. 1988.

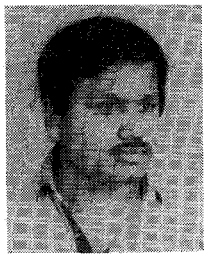

Uttam S. Ghoshal (M'85) received the B.Tech. degree in electrical engineering from the Indian Institute of Technology, Bombay, in 1983 and the M.S. degree in electrical engineering from the University of California at Los Angeles in 1984. At UCLA, his research dealt with modeling and simulation of charges in MOS structures at low temperatures (< 77 K).

Since December 1984, he has been a member of the technical staff at the Microelectronics and Computer Technology Corporation (MCC) in Austin, TX, where he is engaged in the design of wafer scale interconnects and I/O circuits for high-speed digital applications. Since the beginning of 1988, he has been simulating and comparing the performance of superconducting and normal interconnects in digital applications for the newly formed Superconductivity Program at MCC. His current research interests are in the areas of electromagnetic field theory, high-speed CMOS and BiCMOS I/O circuits, structural problems in interconnect structures, and low-temperature electronics.

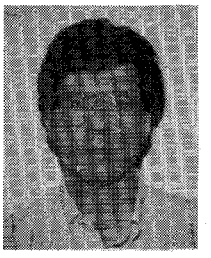

Lawrence N. Smith (M'80) received the Ph.D. degree in physics from the University of Illinois, Urbana, in 1975. From 1975 to 1979, he was a Research Fellow in the Department of Physics at Harvard University. At both these places, he investigated nonequilibrium superconductivity.

From 1979 to 1983, he was a staff member at the Sperry Research Center, working on the characterization, development, and design of the first all-refractory niobium-based IC process for producing Josephson logic. From 1983 to 1984, he was a staff member at the M.I.T. Lincoln Laboratories, where he was responsible for the design of a superconductive time-integrating correlator. In 1985, he joined the Packaging/Interconnect Program at MCC, Austin, TX. He currently is manager of the Interconnect Technology Satellite, which focuses on the design, process development, bonding, and test of high-density wafer-scale copper polyimide multichip substrates. He also participates in the newly created Superconductivity Program, investigating applications of the high-temperature oxide superconductors.

Dr. Smith is the author of more than 25 papers and holds eight patents, with several more in preparation. He is a member of the American Physical Society.